

# Flammability of Nanocomposites – Effects of the Shape of Nanoparticles<sup>#</sup>

Takashi Kashiwagi\*

Fire Science Division, National Institute of Standards and technology  
Gaithersburg, MD 20899-8665 USA

## 1.Introduction

There is a high level of interest in using nanoscale reinforcing fillers for making polymeric nanocomposite materials with exceptional properties[1,2,3]. Nanocomposites are particle-filled polymers where at least one dimension of the dispersed particle is on the nanometer scale. When all three dimensions are of the order of nanometers, we are dealing with true nanoparticles, such as spherical silica, having an aspect ratio of 1. Another type of nanocomposite is characterized by particles having only one dimension on the nanometer scale. In this case, the filler is present in the form of sheets/layers, such as layered silicate or graphite, that are one to a few nanometers thick and hundreds to thousands of nanometers in the other two dimensions. At present, the most common approach for an improvement in flammability is the use of layered silicates having large aspect ratios. When two dimensions are on the nanometer scale and the third is larger, forming an elongated structure, we speak of nanotubes, whiskers, or rods with a high aspect ratio.

An improvement in flammability properties of polymers has been obtained with nanoscale additives and these filled systems provide an alternative to conventional flame retardants. It is important to explore how the asymmetry (aspect ratio) and other geometrical effects of nanoparticle additives influence the flammability properties of polymer nanocomposites. This paper describes flammability properties of nanocomposites based on the three different shapes of nanoscale additives such as nanosilica, clay, and carbon nanotube. The dispersion of the nanoscale particles, the sample behavior during gasification, and the shape and the structure of the sample residues after a gasification test are described as are the flammability characteristics of each nanocomposite based on the different shapes of nanoscale particles.

## 2.Flammability Measurement

Evaluation of flammability properties was achieved using the Cone calorimeter which was designed and built at NIST(ASTM E 1354-92). Aluminum foil was wrapped around the sample, except on the irradiated surface, to form a sample container instead of using the standard, heavy metal container. The tests were performed either at an incident radiant flux of 40 kW/m<sup>2</sup> or at 50 kW/m<sup>2</sup> in air. Heat release rate and mass loss rate are reproducible to within ± 10%. Another device, a radiative gasification instrument similar to the Cone calorimeter, was used to observe the gasification behavior and to measure mass loss rate of the sample in a nitrogen atmosphere (no burning) at 40 kW/m<sup>2</sup> or at 50 kW/m<sup>2</sup>. A more detailed discussion of

---

<sup>#</sup> This work was carried out by the National Institute of Standards and Technology(NIST), an agency of the US government, and by statute is not subject to copyright in the United States.

\* [takashi.kashiwagi@nist.gov](mailto:takashi.kashiwagi@nist.gov), Tel:(301)975-6699, FaxⓈ301)975-4052.

the device is given in our previous study[4]. The unique advantages of this device are twofold: the first is that the results obtained from it are based only on the condensed phase processes due to the absence of any gas phase oxidation reactions; the second is it enables visual observation of gasification phenomena under a heat flux similar to that of a fire without any interference from a flame.

### 3.Polymer-Nanosilica Nanocomposites

The detailed preparation of the poly(methyl methacrylate) (PMMA)/nanosilica nanocomposites is described in ref. 5. The average diameter of the nanosilica particles used in this study was *ca.* 12 nm. The sample was made by *in situ* polymerization of methyl methacrylate with the presence of nanosilica particles. The dimensions of the disk shaped sample were *ca.* 8 cm diameter and 0.6 cm thick. The number averaged molecular weight of this PMMA, measured by size-exclusion chromatography, was  $147,000 \pm 1,000^{\ddagger}$  and that of the PMMA in the nanosilica composite was  $183,000 \pm 8,000$ . The polydispersities of both samples were  $1.9 \pm 0.1$ . The actual content of silica particles in the PMMA/nanosilica nanocomposite was determined by pyrolysing the sample in air at 900 °C in a muffle furnace. By weighing the white powdery residue, a value of  $13 \% \pm 1 \%$  by mass was found rather than the originally intended value of 10 %.

The two polymerized samples, the PMMA/nanosilica nanocomposite and the pristine PMMA (polymerized with the same procedure as that of the nanocomposite), were transparent as seen in Figure 1. Although the transparency of the samples with nanosilica particles suggests reasonably good dispersion of the particles in the PMMA, TEM and AFM images were taken to examine dispersion at the silica scale. TEM analysis of the PMMA/nanosilica nanocomposite at low magnification shows well dispersed areas and also areas of greater silica particle concentration without clustering. The high magnification TEM image in Figure 2 shows well-dispersed silica spheres. The image analysis of the figure shows a histogram of the particle diameter distribution from 10 nm to 30 nm and an average diameter of 12.4 nm.

Observation of the sequence of events in the gasification of the pristine PMMA sample in a nitrogen atmosphere at a radiant flux of  $40 \text{ kW/m}^2$  (no burning) first revealed the appearance of small bubbles bursting at the sample surface around 15 s after the start of irradiation, followed by a rapid increase in the number of bubbles bursting so that they covered the entire sample surface after about 30 s. Around 120 s, the sample surface acquired the appearance of a fluid with larger bursting bubbles and with slight swelling as shown in Figure 3. More vigorous bubbling appeared for times greater than 120 s and the sample became less viscous (more fluid in appearance). After 240 s, the surface was covered by large bursting bubbles and vigorous bubbling with a very fluid sample continued. At the end of the test, no significant amount of residue was left except a thin, black coating on the container surface.

---

<sup>‡</sup> According to ISO 31-8, the term “molecular weight” has been replaced with “relative molecular mass,” symbol  $M_r$ . The conventional notation, rather than the ISO notation, has been employed for this publication.

The gasification behavior of the PMMA/nanosilica nanocomposite was quite different from that of the above PMMA sample. Many small, bubbles were observed initially, but at about 60 s many white islands appeared on the sample surface with vigorous bursting of small bubbles around the islands. Around 120 s, the islands became darker and irregular as shown in Figure 3 (top right). It appeared that the islands were made of coarse, granular particle clumps. The fractional coverage of the sample surface by the islands continued to increase and a random motion of the granular particle clumps on the sample surface was often observed. At about 300 s, the sample surface was completely covered by coarse, granular particle clumps as shown in Figure 3 (bottom right). Also, the sample surface was slowly receding. At the end of the test, a dark, coarse powdery layer was left in the sample container, as shown in Figure 4. The highly fluid behavior observed for the PMMA sample was not seen for this sample. The mass of the residue was almost the same as that of the initial weight of nanosilica and the thickness of the residual layer at the end of the test was roughly half of the initial sample thickness.

The calculated mass loss rates from the measured sample masses of pristine PMMA and PMMA/nanosilica samples are plotted in Figure 5. The peak mass loss rate of the PMMA/nanosilica nanocomposite is roughly 40 % less than that of pristine PMMA. However, the mass loss rate up to 50 s and the total sample mass loss (integrated values of the mass loss curve) are about the same for both samples. These trends are very similar to those of a low molecular weight PMMA/silica gel sample [6].

The heat release rates of pristine PMMA and the PMMA/nanosilica nanocomposite are shown in Figure 6. The addition of the nanosilica reduced the peak heat release rate of the PMMA sample to roughly 50 % of the pristine PMMA value, but the ignition delay time and the total heat release (integrated values of the heat release rate curve) are about the same for both samples. The trends of the measured mass loss rate (burning rate) curves (not shown) are very close to those of the heat release rate curves and thus the calculated specific heat of combustion (measured heat release rate divided by measured mass loss rate) is  $24 \text{ MJ/kg} \pm 2 \text{ MJ/kg}$  for both types of sample. Furthermore, the trends of the heat release rate curves are very similar to those of the mass loss rate in nitrogen, as shown in Figure 5. The PMMA/nanosilica nanocomposite residue after the cone calorimeter tests was a gray layer consisting of coarse, granular powder accumulated at the bottom of the sample container, which is very similar to that shown in Figure 4.

#### **4. Polymer-Clay Nanocomposites**

Polyamide 6, PA6, was selected as a resin for this study and commercially available PA6/clay samples were used. They were PA6 homopolymer (molecular mass ( $M_w$ ) of about 15,000 g/mol, UBE 1015B<sup>1</sup>), PA6 ( $M_w \approx 15,000$ ) with montmorillonite (MMT) of 2 % by mass (UBE 1015C2), and PA6 ( $M_w \approx 18,000$ ) with MMT of 5 % by mass (UBE 1018C5). They were selected due to their exfoliated clay dispersion in PA6. Sample disks (75 mm diameter and 8 mm thickness) were injection molded. TEM images of the original sample show that the clay

---

<sup>1</sup> Certain commercial equipment, instruments, materials, services or companies are identified in this article to specify adequately the experimental procedure. This in no way implies endorsement or recommendation by the National Institutes of Standards and Technology (NIST).

platelets were fully exfoliated as shown in Figure 7. Note at the position labeled “A” in the figure, two platelets spaced approximately 1.5 nm apart can be seen clearly. However, such close platelets were rare. Wide-angle XRD measurements were conducted to obtain clay particle structure in the sample. A comparison of the XRD data between clay and PA6/clay(5%) sample is shown in Figure 8. The XRD data of the original Na-clay shows many peaks with the d-spacing of about 1.19 nm (at  $2\theta$  of about  $7.44^\circ$ ). However, the PA6/clay(5%) sample shows a sharp peak at  $2\theta$  of about  $21.4^\circ$  corresponding to the  $\gamma$  crystalline phase of PA6 without any peak corresponding to the clay. The results indicate that clay platelets were fully exfoliated in agreement with the results of the TEM images. More detailed discussion of the dispersion of clay platelets in PA6 and further XRD data of collected residues could be found in our previous publication [7].

Observation of the sequence of events in the non-flaming gasification of the PA6 sample without clay first revealed small bubbles of evolved degradation products at the sample surface, followed by the appearance of many large bubbles. About 60 s after the start of irradiation, the size of the bubbles became gradually smaller and around 120 s many small bubbles with few larger size bubbles appeared, as shown in Figure 9. The sample appeared less viscous (more fluid-like) with numerous small bubbles. Shortly after 200 s, some swelling of the sample was observed giving it the appearance of a highly viscous mound. Vigorous bubbling in the very fluid-like upper layer of the sample continued, and the sample surface gradually darkened after 400 s. A very thin, black coating over the bottom of the container was left at the end of the test, as shown in Figure 10. The amount of the residue at the end of the test was less than 1 % of the initial sample mass.

The gasification behavior of the PA6/clay(2%) nanocomposite was initially similar to that of the PA6 sample except that it appeared to be more viscous; it still had the appearance of a viscous fluid. Around 150 s several small, dark floccules appeared on the surface and these grew with time, as shown in Figure 9. However, they never covered the entire sample surface. Numerous small dark floccules were formed together with a few large floccules. The dark crust-like floccules were left at the bottom of the container at the end of the test. The mass of the residue was about 2 % of the initial sample mass. The PA6/clay(5%) nanocomposite appeared to be much more viscous than the PA6 sample during the gasification test but it still formed numerous larger bubbles. Around 100 s after the start of irradiation, a thin, black ring (not continuously connected) appeared at the perimeter of the sample and this ring moved toward the center of the sample then collapsed to form a large black clump around 150 s. More black floccules appeared near the perimeter of the sample and moved gradually toward the center and formed larger rough-surface floccules. This can be seen in the images at 200 s in Figure 9. Vigorous bubbling of evolved degradation products was observed over that portion of the sample surface which was not covered by the black floccules. The floccules gradually grew and were left at the bottom of the container at the end of the test. The mass of the residue was about 5 % of the initial sample mass. A picture of the residue collected after the test is shown for each sample in Figure 10. These residues look like a carbonaceous char and are brittle and fragile. The PA6/clay(5%) nanocomposite generated more residue of the black floccules than the PA6/clay(2%) nanocomposite. Similar black floccules were also observed in the residues of the burned samples tested in the cone calorimeter. These pictures indicate that the formation of the protective, black floccules and their coverage over the sample surface are desirable as a means of

reducing the exposure of the molten polymer to external radiant flux or to heat feedback from a flame. For most effective FR performance, they need to cover the entire sample surface in order to fully shield/protect the polymer melt.

The ideal structure of a protective surface layer (consisting of clay particles and some char) is net-like and has sufficient physical strength not to be broken or disturbed by bubbling. The protective layer should remain intact over the entire burning period. Although the PA6/clay nanocomposites studied here formed such a protective layer covering a part of the sample surface, it was reported that the polystyrene (PS)/clay nanocomposite sample formed such a protective layer covering the entire sample surface, as shown in Figure 11[8]. This could be due to enhanced formation of char from PS by the addition of clay. However, several large cracks were observed in the residues of this particular PS/clay nanocomposite sample.

Heat release rate curves of the three PA6-based samples are shown in Figure 12. The results show that the nanocomposite samples have a slightly increased ignition delay time and a significantly peak heat release rate in comparison to pristine PA6. The greater the clay content the lower the heat release rate corresponding to the surface coverage by the floccule layer. There is no significant reduction in total heat release due to the nanocomposites for the levels of clay content used in this study. This indicates that the nanocomposites burn more slowly, but they burn nearly completely. The mass loss rate curve of each sample (not shown) is proportional to the heat release rate curve. Thus, the specific heat of combustion obtained from the heat release rate divided by mass loss rate is  $30 \text{ kJ/g} \pm 2 \text{ kJ/g}$  for all three samples. This unchanged specific heat of combustion implies that the observed reduction in heat release rate (and mass burning rate) tends to be due to chemical and physical processes mainly in the condensed phase rather than in the gas phase.

## 5. Polymer-Carbon Nanotube Nanocomposites

A detailed description of the preparation of poly (propylene) (PP)/multi-walled carbon nanotube (MWNT) nanocomposites is given in ref. [9]. The nanocomposites were prepared by melt blending without any compatibilizer or organic treatment. All samples were compression molded to make 75 mm diameter by 8 mm thick disks. The distribution of the nanotubes in the sample was examined by two different methods and magnifications. One used scanning electron microscopy (SEM). A SEM picture of the recovered MWNTs after solvent was removal of of PP from a PP/MWNT (1 %) nanocomposite is shown in Figure 13. Although it shows well dispersed MWNTs *implying* good dispersion in the PP/MWNT nanocomposite, more direct observation and a larger observation area of the dispersion of MWNTs in the PP/MWNT samples are preferred. The second method used optical microscopy; an image of the PP/MWNT(1%) is shown in Figure 14. It shows globally well-dispersed nanotubes in PP and also a wide range of diameters and lengths of nanotubes as shown in Figure 13.

The physical behavior of the PP/MWNT nanocomposites was significantly different from that of pristine PP during the gasification test. As shown in Figure 15(a), the pristine PP sample behaved like a liquid with a fine froth layer generated by the bursting of numerous small bubbles at the sample surface. No char was left at the end of the test. However, all PP/MWNT samples

tested in this study behaved like a solid without any visible melting except at the very beginning of the test and the shape of the sample did not significantly change during the test. A picture of the residue of the PP/MWNT(1%) nanocomposite is shown in Figure 16. The shape of the residue was nearly the same as the original sample except for slight shrinkage. No cracks were observed in any residue of the PP/MWNT nanocomposites studied in this paper. The networked floccule residues of the PP/MWNT samples covered the entire sample surface and extended to the bottom of the residue as shown in Figure 17. The floccule residue was porous, but had physical integrity and did not break when lightly picked at by one's fingers. The mass of the floccule residue was very close to the initial mass of carbon nanotubes in the original nanocomposite. This indicates that the networked floccule did not enhance char formation from PP.

A comparison of heat release rate curves among the three samples is shown in Figure 18. The results show that the heat release rates of the PP/MWNT nanocomposites are much lower than that of pristine PP even though the amount of MWNT in PP is quite small. The total heat release, the integral of the heat release rate curve over the duration of the experiment, is about the same for the three samples. The curves of the mass loss rate per unit surface area for the three samples are very similar to those of the heat release rate. Since the specific heat of combustion value is calculated by dividing measured heat release rate with measured mass loss rate, this indicates that the specific heat of combustion is about the same for the three samples. The calculated specific heat of combustion of each sample is  $43 \pm 1$  MJ/kg. The above results indicate that the PP/MWNT nanocomposites burn much slower than PP but they all burn nearly completely. These observations are similar to those made with clay-nanocomposites and with composites made by the addition of nanoscale silica in PMMA, as described above. This indicates that the observed FR performance of the PP/MWNT nanocomposite is mainly due to chemical and/or physical processes in the condensed phase instead of in the gas phase.

## Discussion

The heat release rate curves of the three different types of nanocomposites show that large reduction in heat release rate is achieved in the following decreasing order: polymer-MWNT nanocomposites, polymer-clay nanocomposite, and polymer-nanosilica nanocomposites. The residues of these nanocomposites show (1) a low density network-like protective layer covering the entire sample surface without any cracks for the PP/MWNT nanocomposite, (2) floccular islands consisting of clay and char for the PA6/clay nanocomposites, and (3) the formation of coarse, granular particulate clumps for the PMMA/nanosilica nanocomposites. This suggests that the formation of a continuous network-like protective layer which covers the entire sample surface is critically needed to significantly reduce heat release rate with only a small mass of these nanoscale particles. Some polymer/clay nanocomposites can form such a layer with the PS/MMT nanocomposites [8] and the PP/polypropylene-grafted maleic anhydride (PP-g-MA)/MMT nanocomposites [10]. However, their residues were slightly brittle and were cracked. Therefore, it appears that a higher clay content (5 %-10 %) in polymers is needed to obtain a similar amount of reduction in heat release rate as that of the PP/MWNT (1%) nanocomposite.

The formation of a continuous, low-density network-structured protective layer is easiest with high aspect ratio nanoscale particles. The aspect ratio of the nanosilica in PMMA is about 1 and coarse, granular particulate clumps, probably coagulated silica particles, were formed instead of a network structure. The effects of aspect ratio for plate-like clay particles on the heat release rate of polymer/clay nanocomposites were determined using three different clays; synthetic mica (aspect ratio of roughly one thousand), MMT (about 100), and synthetic hectolite (few hundreds). The PP/PP-g-MA/clay nanocomposites (all had 7.7 % clay by mass) were prepared by melt mixing and the mass loss rate of each sample was measured in nitrogen in the gasification test at 50 kW/m<sup>2</sup>. The sample was a 10 cm x 10 cm x 0.3 cm thick plate. The results are shown in Figure 19. The lowest mass loss rate was observed for the sample with synthetic mica which generated a significantly lower mass loss rate than those with MMT and synthetic hectolite. There was little difference in mass loss rate between the sample with MMT and with synthetic hectolite. The pictures of the residues of the four samples after the tests are shown in Figure 20. The surface of the residue of the sample with synthetic mica shows a relatively smooth surface without any large cracks. However, the two samples with the other two clays show large cracks (in particular, with synthetic hectolite). Melting and vigorous bubbling were observed in the large cracks during the test. Similar behavior was observed at the exposed sample surface of PA6/clay, as shown in Figure 9. The different types of clay in the PP/PP-g-MA/clay nanocomposites formed the slightly different structure of the protective layer during the test. It appears that this was caused by the difference in aspect ratio among the three clays. Nanoscale particles with higher aspect ratio tend to form a network-like structure of a protective layer covering the entire surface without any significant cracks.

The dispersion of the clay particles in a polymer/clay nanocomposite has significant effects on the reduction in heat release rate. If the clay particles are not well dispersed in the nanocomposite, no significant reduction in heat release rate has been reported for the PS/MMT sample [8]. A similar trend was recently observed with polymer/MWNT nanocomposites. Therefore, nanoscale particles in a polymer nanocomposite should be well dispersed to obtain the maximum performance in reducing heat release rate.

Nanocomposites generally reduce heat release rate, in particular the peak heat release rate. However, they tend to have slightly shorter ignition delay times (or no significant increase in ignition delay) and about the same total heat release as those of pristine polymers. As previously described in this paper, nanocomposites tend to burn slowly and nearly completely. Although the use of a small quantity of nanoscale particles in polymers to form nanocomposites could be one of the alternatives to conventional flame retardants, nanocomposites need further improvements for increasing ignition delay time and for reducing total heat release.

## **Conclusion**

Nanocomposites based on three different shapes of nanoscale particles, sphere (silica), plate (clay), and tube (carbon nanotube), were prepared and the dispersion of the particles in the nanocomposites was confirmed by various techniques using TEM, SEM, optical microscopy, and XRD. Their flammability properties were measured by using a Cone calorimeter and a radiative gasification apparatus in nitrogen. The residues of these nanocomposites after the gasification test were collected and the shape and the structure of the residues were examined. The results

show that the reduction in heat release rate is achieved in the order: carbon nanotubes, clay platelets, and silica spheres providing that these particles are well dispersed in the sample. It appears that the particles having higher aspect ratio tend to form an effective protective layer consisting of network-structured floccule which covers the entire sample surface without forming any cracks during burning. The formation of such a layer is critical to obtain low heat release rate from nanocomposites.

### Acknowledgement

This paper is based on the results obtained from many different projects, as described in refs. 6, 7, and 8, with the collaboration of many people. The author would like to thank Richard Harris, John Shields, Alexander Morgan (currently at Dow Chemical Co.), Kathryn Butler, and Jeffrey Gilman at the Fire Science Division for their collaboration, Xin Zhang and Robert Briber at the Department of Materials Science and Engineering of University of Maryland for the collaboration with the PA6/clay work, Jenny Hilding and Eric Grulke at the Department of Chemical and Materials Engineering of University of Kentucky for their collaboration with the PP/MWNT work, Joseph Antonucci, Semen Kharchenko and Jack Douglas of the Polymers Division of NIST for the preparation of PMMA/nanosilica nanocomposites and valuable discussions about the properties of polymer nanocomposites, and finally Koichi Iwasa at Sekisui Chemical Co. for the collaboration with PP/PP-g-MA/clay work.

### Reference

- <sup>1</sup> Kojima Y, Usuki A, Kawasumu M, Okada A, Fukushima Y, Kurauchi T, Kamigaito O, *J. Mater. Res.* 1993;8:1185-1189.
- <sup>2</sup> Giannelis EP, *Adv. Mater.* 1996;8:29-35.
- <sup>3</sup> Wang Z, Pinnavaia TJ, *Chem. Mater.*, 1998;10:1820-1826.
- <sup>4</sup> Austin PJ, Buch RR, Kashiwagi T, *Fire Mater.* 1998, 22, 221-237.
- <sup>5</sup> Kashiwagi T, Morgan AB, Antonucci JA, VanLandingham MR, Harris RH Jr, Awad WH, Shields JR, *J. Appl. Polym. Sci.* 2003;89:2072-2078.
- <sup>6</sup> Kashiwagi T, Shields, JR, Harris RHJr, Davis RD. *J. Appl. Polym. Sci.* 2003;87:1541-1553.
- <sup>7</sup> Kashiwagi T, Harris RH Jr, Zhang X, Briber RM, Cipriano BH, Raghaven SR, Awad WH, Shields JR, to appear in *Polymer*.
- <sup>8</sup> Morgan AB, Harris RHJr, Kashiwagi T, Chyall LJ, Gilman JW. *Fire Mater.* 2002;26:247-253.
- <sup>9</sup> Kashiwagi T, Grulke E, Hilding J, Harris RH Jr, Awad WH, Douglas J, *Macromol. Rapid Commun.* 2002;23:761-765.
- <sup>10</sup> Morgan AB, Kashiwagi T, Harris RH, Campbell JR, Shibayama K, Iwasa K, Gilman JW, Fire and Polymers ed. Nelson GL, and Wilkie CA, 2001, ACS Sym. Series 797:9-23.

## Figure Captions

Figure 1. Pictures of the PMMA/nanosilica nanocomposite sample (left) and the PMMA sample (right).

Figure 2. TEM image of the PMMA/nanosilica nanocomposite (left), analyzed image (middle), and a histogram distribution of diameter (right).

Figure 3. Selected sequence of video images of gasification phenomena of PMMA and PMMA/nanosilica samples in  $N_2$  at  $40 \text{ kW/m}^2$ . Left column: PMMA and right column: PMMA/nanosilica, time at 120 s, 240 s, and 300 s from top. The container of the PMMA sample was held by four small wires to avoid its movement.

Figure 4. Picture of the residue consisting of granular, coarse particles after the gasification test in nitrogen at  $40 \text{ kW/m}^2$ .

Figure 5. Effects of nanosilica addition on mass loss rate of PMMA at  $40 \text{ kW/m}^2$  in nitrogen.

Figure 6. Effects of nanosilica addition on heat release rate of PMMA at  $40 \text{ kW/m}^2$ . The dashed lines were the results of three replica of nanocomposites made at three different times.

Figure 7. TEM image of the PA6/clay(5%) sample.

Figure 8. XRD of  $Na^+$  clay and PA6/clay(5%).

Figure 9. Selected video images of the three samples at 100 s, 200 s, and 400 s in nitrogen at  $50 \text{ kW/m}^2$ .

Figure 10. Residue pictures at the end of the gasification tests in  $N_2$  at  $50 \text{ kW/m}^2$ .

Figure 11. Selected video images of gasification behavior of PS and PS/MMT(5%) nanocomposite in nitrogen at a flux of  $50 \text{ kW/m}^2$ . The extensive carbonaceous char formation can clearly be observed in the nanocomposite (right) samples.

Figure 12. Effects of clay content on heat release rate of PA6.

Figure 13. SEM picture of MWNT dispersion in the PP/MWNT(1%) nanocomposite after solvent removal of PP.

Figure 14. Optical microscopy image of MWNT/PP(1%) nanocomposite in the melt.

Figure 15. Sample behavior in the gasification test at  $50 \text{ kW/m}^2$  in nitrogen, (a) PP, and (b) PP/MWNT(1%).

Figure 16. Picture of the residue of PP/MWNT(1%) after the gasification test in nitrogen at  $50 \text{ kW/m}^2$ .

Figure 17. The cross section of the residue of the PP/MWNT (1%) nanocomposite shown in Figure 15 (b).

Figure 18. Comparison of heat release rate curves among PP and PP/MWNT nanocomposites at 50 kW/m<sup>2</sup>.

Figure 19. Effects of clay type on mass loss rate of PP(92.3%)/PPgMA(7.7%) and PP(84.6%)/PPgMA(7.7%)/Clay(7.7%) samples in nitrogen at 50 kW/m<sup>2</sup>.

Figure 20. Effects of clay type on the surface pattern of the residues of PP(92.7%)/PPgMA(7.7%) and PP(84.7%)/PPgMA(7.7%)/Clay(7.7%) samples after gasification test in nitrogen at 50 kW/m<sup>2</sup>



Figure 1.

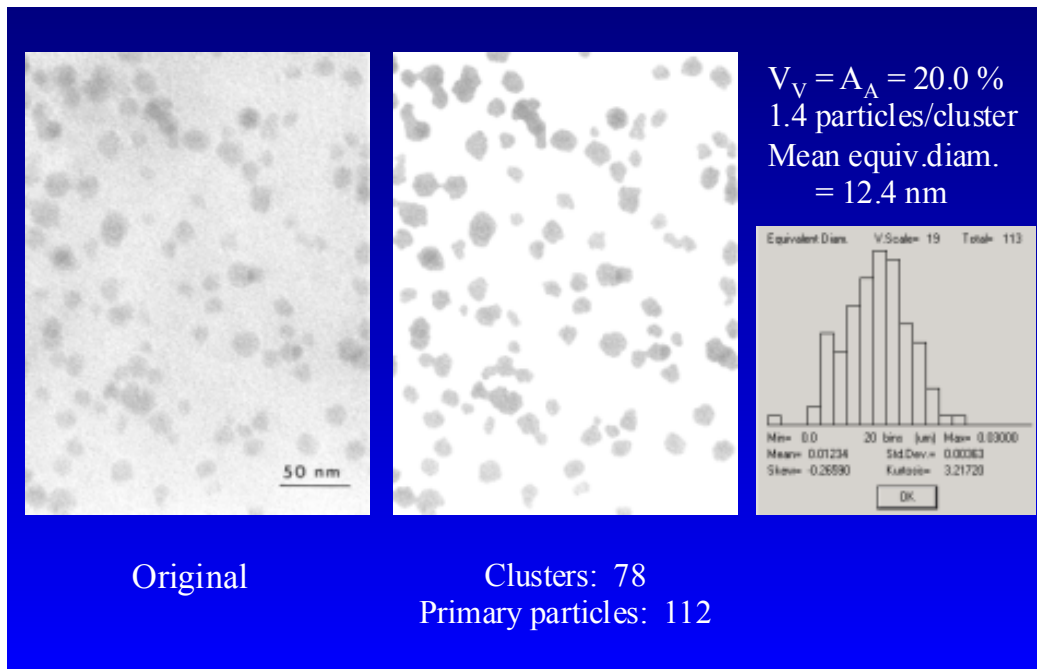


Figure 2.

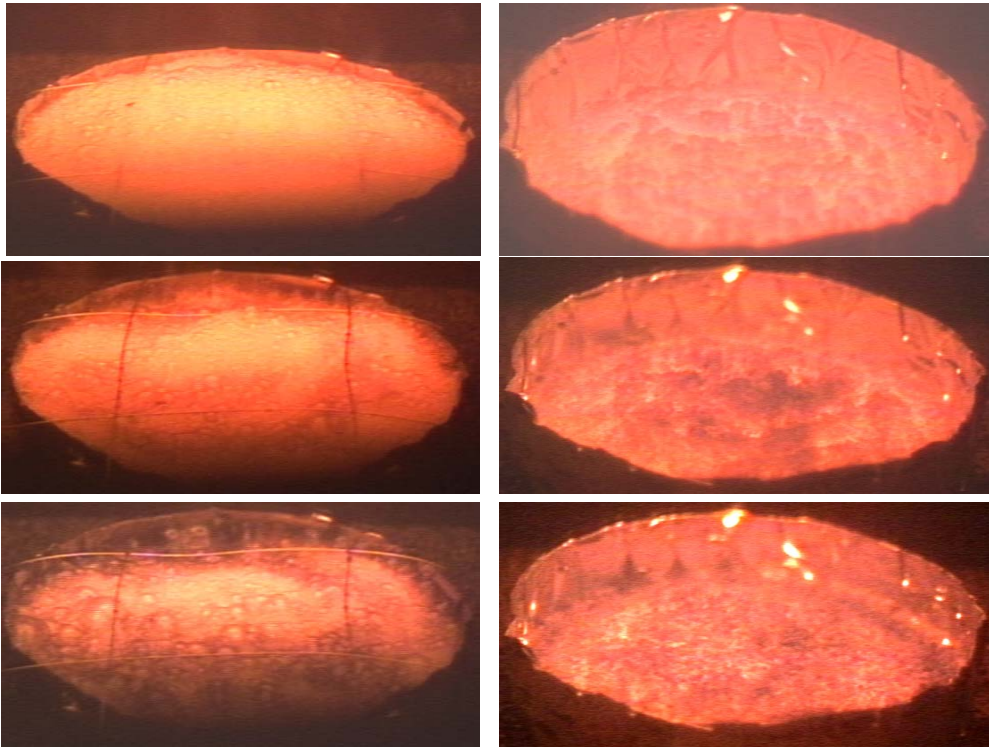


Figure 3.

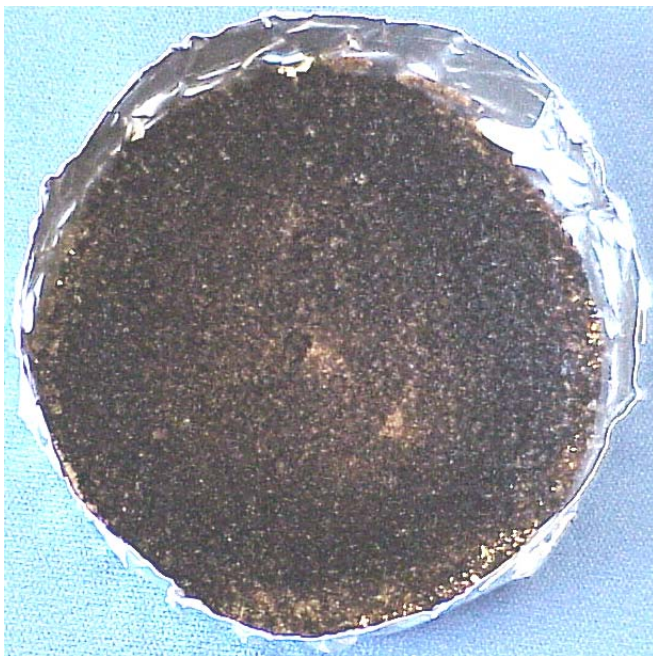


Figure 4.

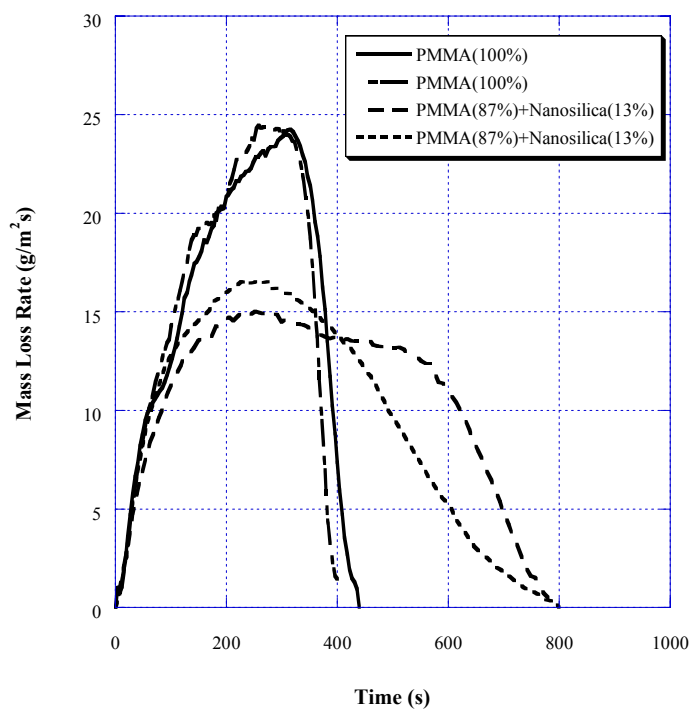


Figure 5

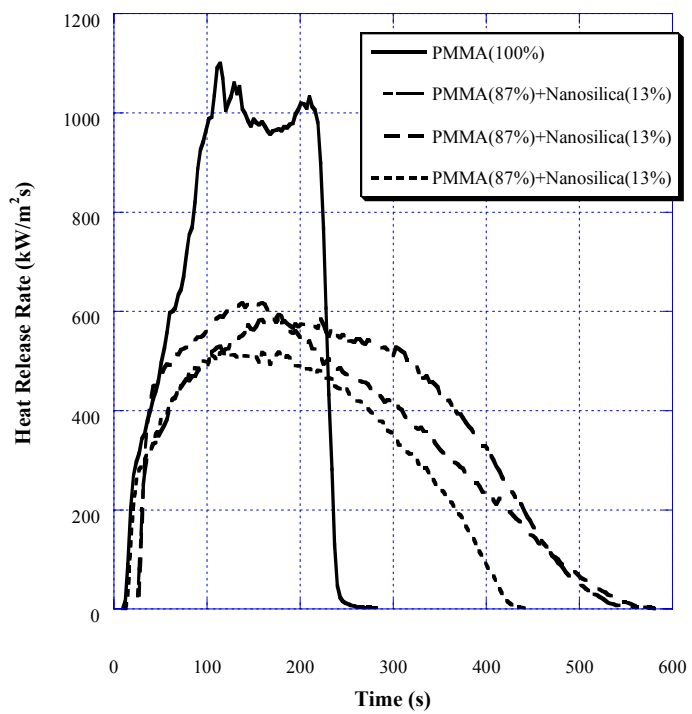


Figure 6.

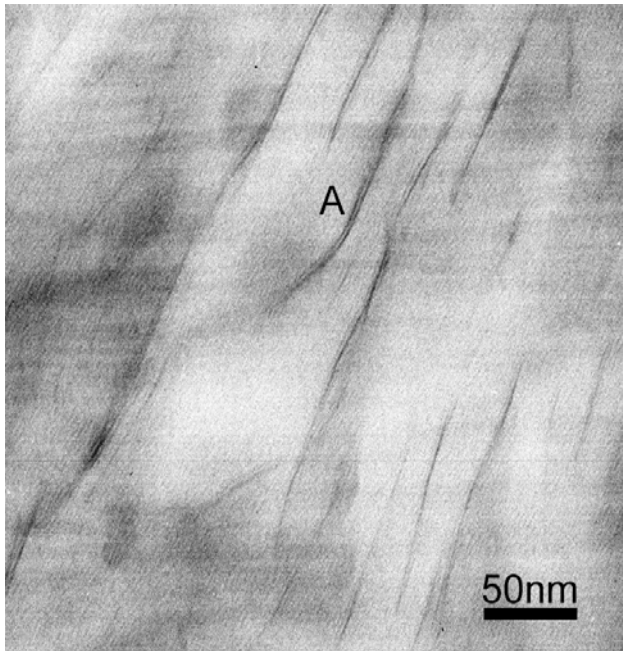


Figure 7.

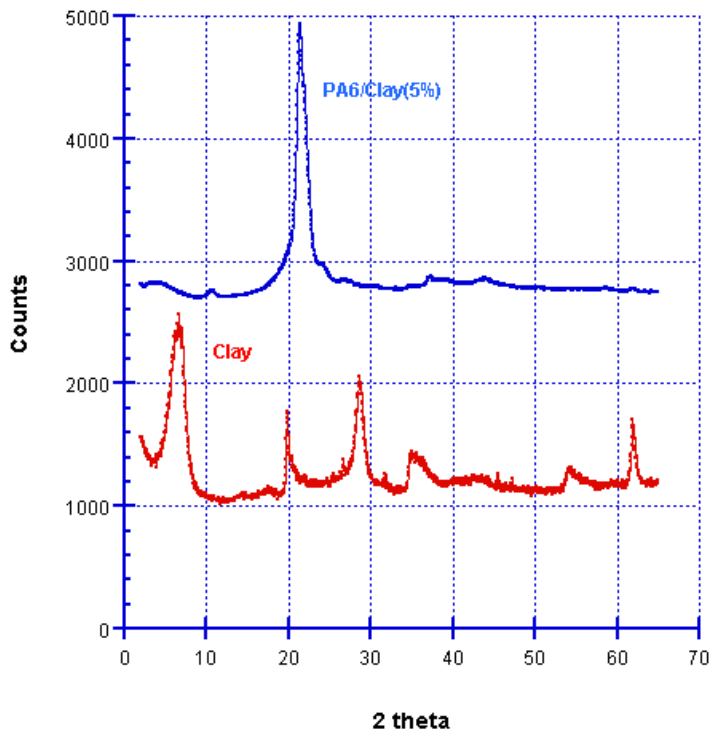
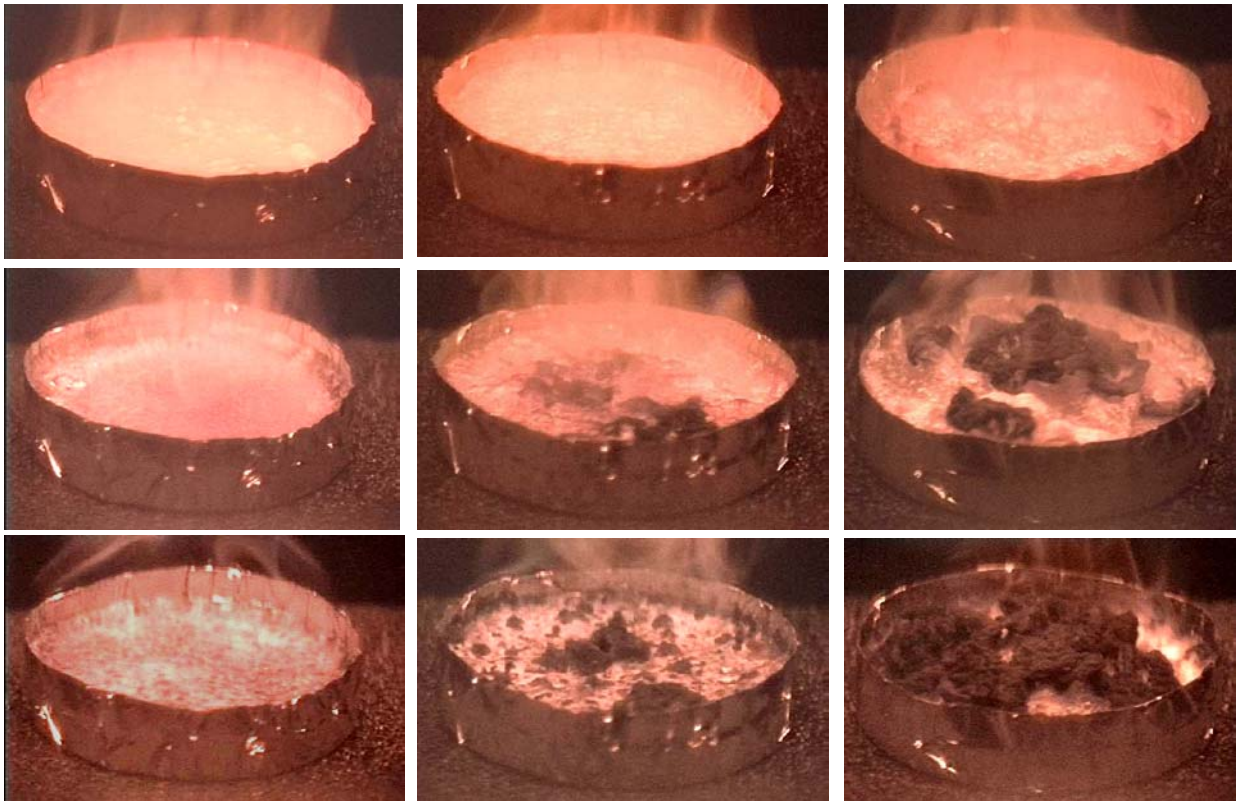


Figure 8.



PA6

PA6/Clay(2%)

PA6/Clay(5%)

Figure 9.



PA6

PA6/Clay(2%)

PA6/Clay(5%)

Figure 10.

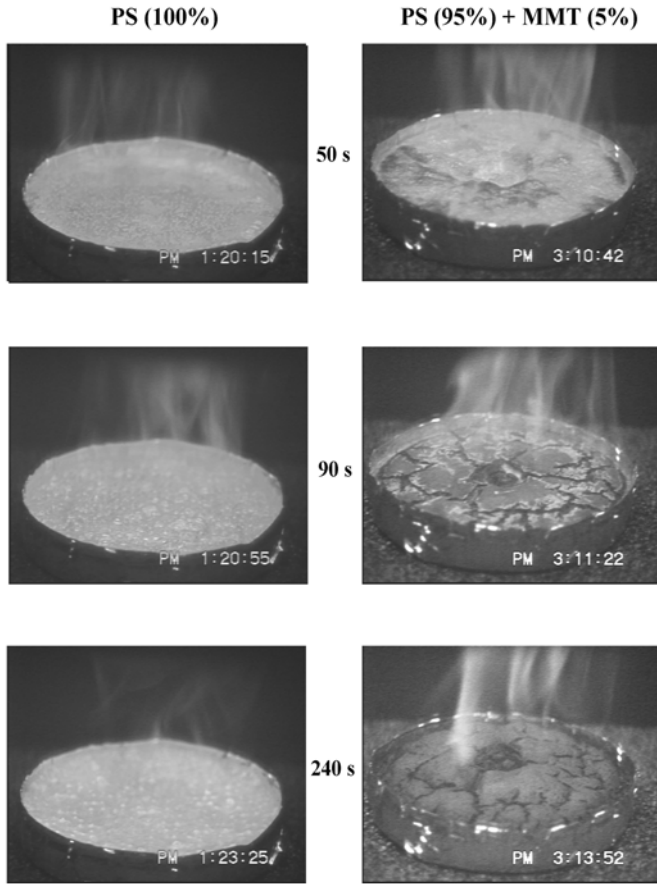


Figure 11.

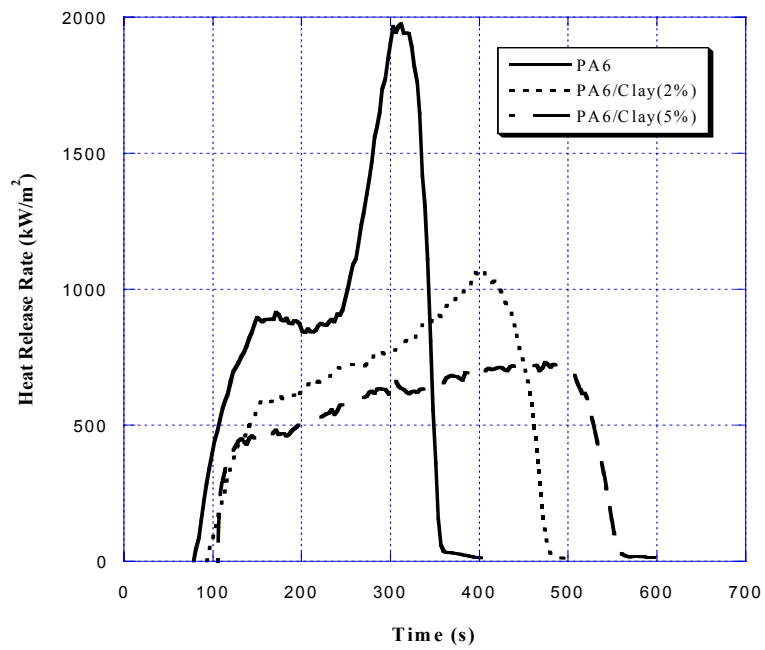


Figure 12. (8 mm thick) at 50 kW/m<sup>2</sup>.

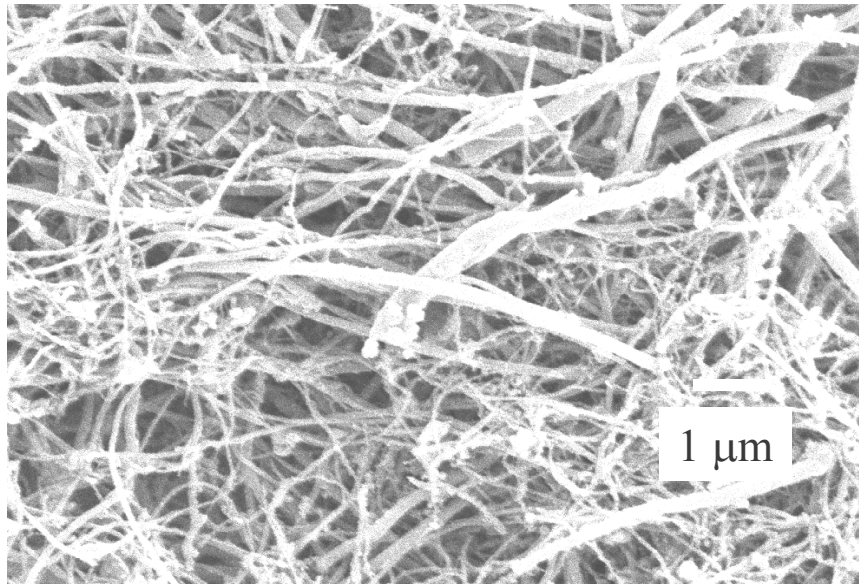


Figure 13.

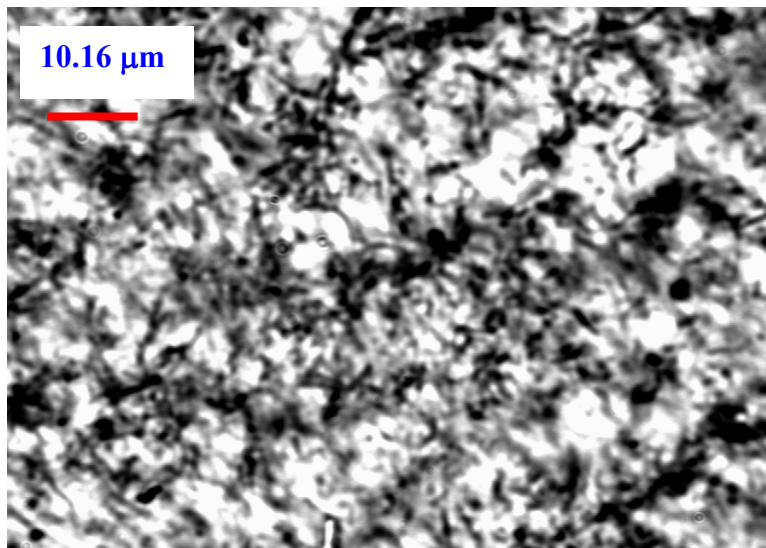
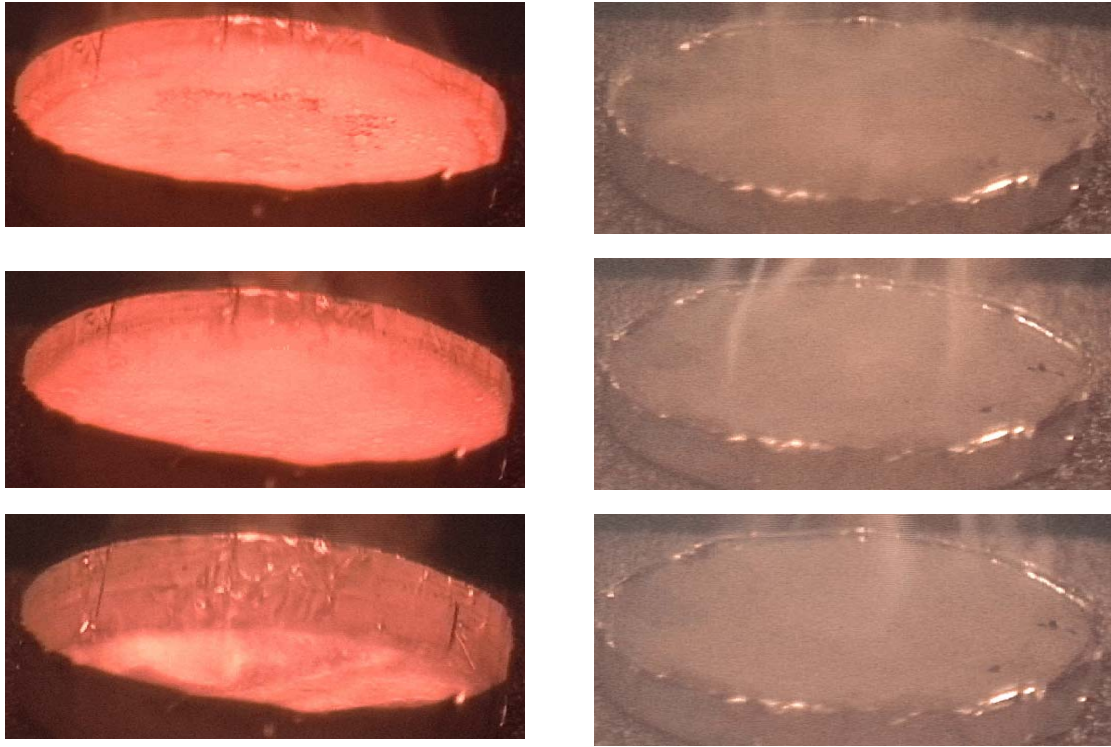


Figure 14.



(a)

(b)

Figure 15.

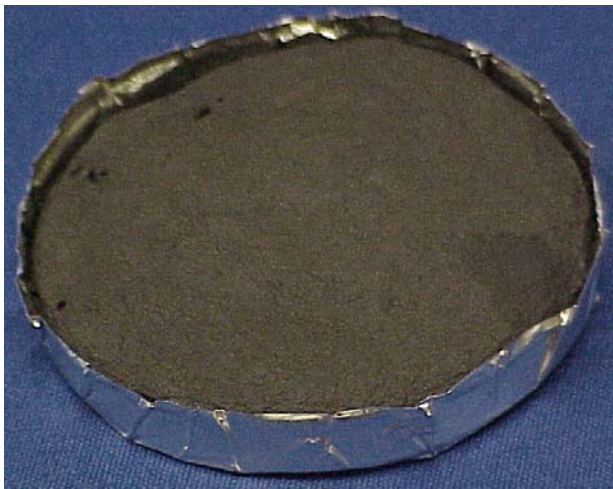


Figure 16.

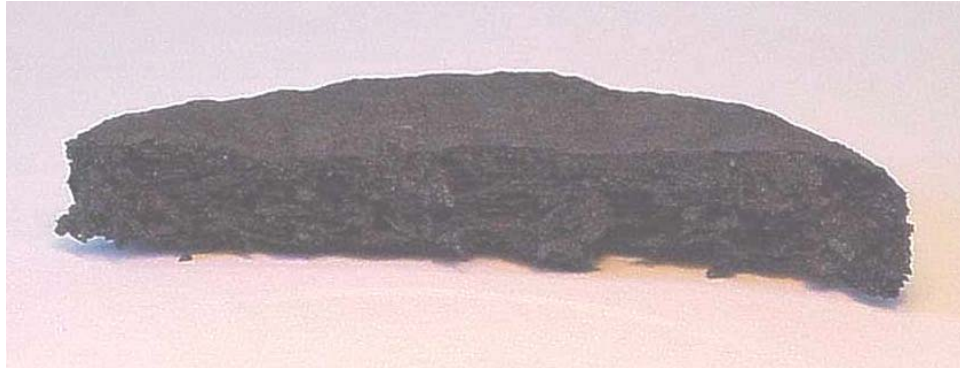


Figure 17.

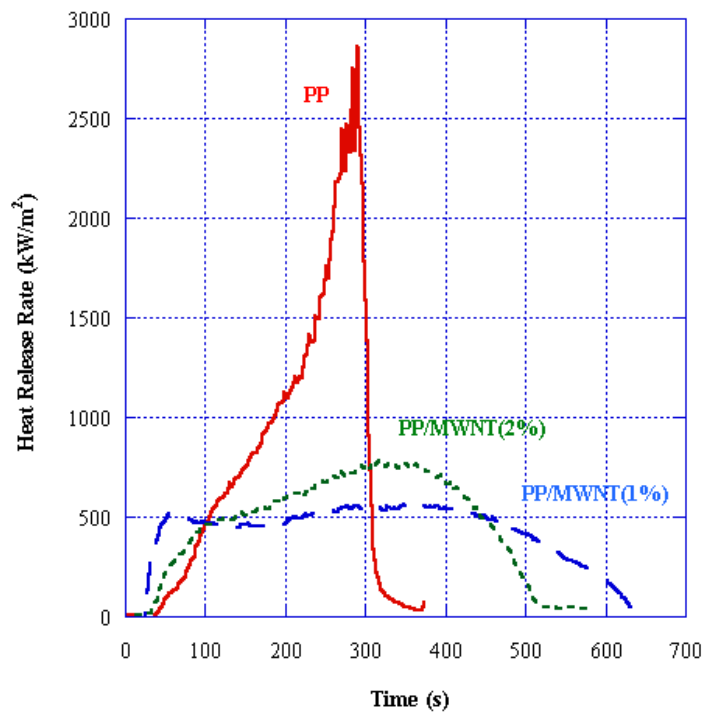


Figure 18.

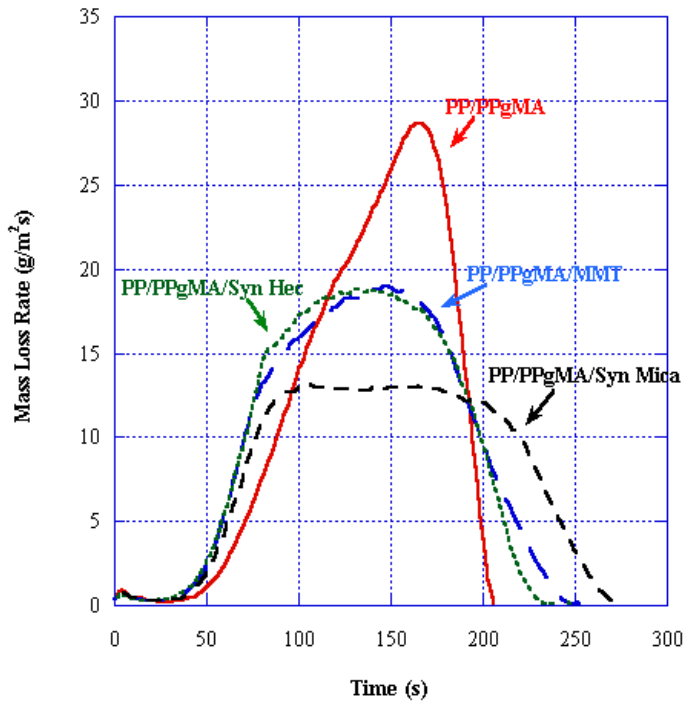


Figure 19.



**PP/PPgMA**



**PP/PPgMA/MMT(7.7%)**



**PP/PPgMA/Syn. Hect.(7.7%)**



**PP/PpgMA/Syn. Mica(7.7%)**

Figure 20